

Disturbance reduction system: testing technology for precision formation control

W. M. Folkner^a, S. Buchman^b, R. L. Byer^b, D. DeBra^b, C. J. Dennehy^c, M. Gamero-Castaño^d, J. Hanson^c, V. Hruby^d, G. M. Keiser^b, A. Kuhnert^a, F. L. Markley^c, M. Houghton^c, P. Maghami^c, D. Miller^a, S. Prakash^c, R. Spero^a

^aJet Propulsion Laboratory, California Institute of Technology, Pasadena, CA 91109

^bHansen Laboratories, GP-B, Stanford University, Stanford, CA 94305

^cBusek Co., Inc., 11 Tech Circle, Natick, MA 01760

^dGoddard Space Flight Center, Greenbelt, MD 20771

^eCrossTrac Engineering,

ABSTRACT

The Disturbance Reduction System (DRS) is a space technology demonstration within NASA's New Millennium Program. DRS is designed to validate system-level technology required for future gravity missions, including the planned LISA gravitational-wave observatory, and for formation-flying interferometers. DRS is based on a freely floating test mass contained within a spacecraft that shields the test mass from external forces. The spacecraft position will be continuously adjusted to stay centered about the test mass, essentially flying in formation with the test mass. Colloidal microthrusters will be used to control the spacecraft position within a few nanometers, over time scales of tens to thousands of seconds. For testing the level of acceleration noise on the test mass, a second test mass will be used as a reference. The second test mass will also be used as a reference for spacecraft attitude. The spacecraft attitude will be controlled to an accuracy of a few milliarcseconds using the colloidal microthrusters. DRS will consist of an instrument package and a set of microthrusters, which will be attached to the European Space Agency's SMART-2 spacecraft with launch scheduled for August 2006.

Keywords: formation flying, colloidal microthrusters, disturbance reduction

1. DISTURBANCE REDUCTION SYSTEM OVERVIEW

The Disturbance Reduction System (DRS) is designed to validate system-level technology required for two types of future missions: measurements of planetary gravity and of cosmic gravitational waves, and precision formation-flying interferometers. The validated technology will feed directly into the LISA gravitational-wave observatory, the MAXIM X-ray interferometer mission, and several other missions within the NASA roadmap. The DRS is based on the concept of a freely floating test mass contained within a spacecraft that shields the test mass from external forces. The test mass will ideally follow a trajectory determined only by the local gravitational field. The spacecraft position must be continuously adjusted to stay centered about the test mass, essentially flying in formation with the test mass. The DRS performance is characterized by the extent to which unwanted accelerations appear on the test mass and the accuracy with which the spacecraft is centered on the test mass. The project goals are to demonstrate acceleration levels below 3×10^{-14} m/s²/√Hz and position control to 10 nm/√Hz over a frequency range of 1 mHz to 10 mHz.

In order to measure the level of accelerations appearing on the test mass, its trajectory must be compared with a reference trajectory. For DRS, the reference is provided by a second identical test mass located within the same instrument assembly. Being located in the same spacecraft, the second test mass must be controlled at frequencies below the measurement bandwidth to keep its position relative to the primary test mass, while being free of control forces within the measurement bandwidth to provide a reference for acceleration measurements. The position of the second test mass will be measured with respect to the spacecraft. To keep the second test mass as free from external disturbances as possible within the measurement bandwidth, the spacecraft attitude will be controlled to follow the motion of the second test mass relative to the first.

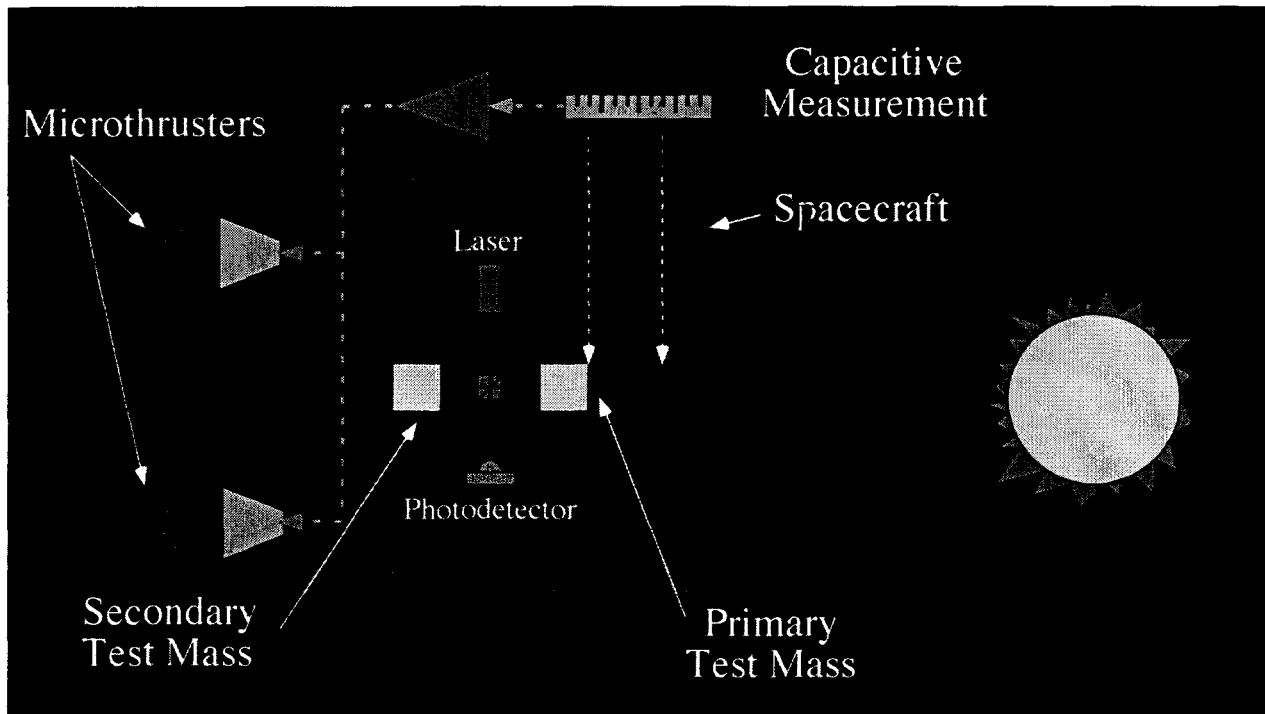


Figure 1 Artist's concept of the Disturbance Reduction System

The functionality of the DRS is indicated in Figure 1. The two cubical test masses are enclosed within cubical cavities of housings rigidly attached to the body of the spacecraft. Electrodes on the inner faces of the housings are used to measure the position and orientation of the test masses with respect to the housings. This capacitive sensing mechanism has been used in many previous missions, including the Triad drag-free demonstration¹ and on Gravity Probe-B². A laser interferometer will measure changes in distance between the two test masses to infer the residual acceleration noise. The largest external force acting on the spacecraft is the solar light pressure, which is about $10 \mu\text{N}$ in magnitude (assuming a 1 m^2 area for the spacecraft). Colloidal microthrusters will be fired to oppose the solar radiation pressure, operating within a control loop designed to keep the spacecraft centered about the test masses.

The spacecraft position control requirements are derived both from the desire to demonstrate the ability to control spacecraft position to a fraction of a wavelength of light and to minimize variation on the forces exerted on the test masses from the gravitational attraction of the spacecraft components and from spacecraft magnetic and electric fields. In order to control the position of the spacecraft with an accuracy of $10 \text{ nm}/\sqrt{\text{Hz}}$, the position of the test mass with respect to its housing will be measured with an accuracy of $3 \text{ nm}/\sqrt{\text{Hz}}$, and the thrusters will have output controlled with a step size of $0.1 \mu\text{N}$ and a stability of $0.1 \mu\text{N}/\sqrt{\text{Hz}}$. The spacecraft attitude control accuracy, in rotation about the two axes perpendicular to the direction between the two test masses, is determined by the accuracy with which the position of the second test mass is measured divide by the distance between test masses, which is nominally 30 cm .

The use of the freely-floating test masses as position and attitude references allows for a demonstration of the spacecraft control system to a high degree of accuracy. The test mass control ensures that the spacecraft disturbances will be very low. For a separated-spacecraft interferometer mission, the control would be based on a spacecraft-spacecraft metrology system which is not included as part of the DRS but could be used with the same thrusters and similar control algorithms to achieve a formation control at the nanometer level. For single-aperture telescope, the microthrusters could be used with a pointing reference to provide a very stable attitude control.

The DRS sensors and thrusters are described briefly below, followed by some preliminary analysis of expected control performance.

2. GRAVITATIONAL REFERENCE SENSORS

Each Gravitational Reference Sensors (GRS) consists of a test mass that floats freely in its housing. The separation between the test mass and its housing in all six degrees of freedom is monitored by non-contacting capacitor plates fixed to the housing. The largest disturbances to the inertial trajectory of a craft in space (radiation pressure, residual gas drag, and particulate impacts) are cancelled by the basic concept of a drag reduction system. The final performance of the system will be limited by a number of smaller disturbances. These disturbances fall into three categories: 1) variations in the gravitational potential at the test-mass location, 2) momentum transfer to the test mass by residual gas and cosmic radiation particles, and 3) variations of the electromagnetic fields at the test-mass location. The main gravitational fluctuations are due to the thermal distortion of the spacecraft and to the relative displacement of the test-mass with respect to the spacecraft. Improving the thermal shielding, using materials with low temperature coefficient, and maximizing the symmetry of the mass distribution of the spacecraft will reduce the thermal distortion effects. Reducing the gravity gradient and displacement of the test mass minimizes the gravity noise caused by spacecraft displacement. For reasonable space-experimental pressures, $10^{-7} - 10^{-6}$ Pa at 250 – 300 K, the forces caused by residual gas impacts are dominant compared to forces produced by cosmic radiation, though well below the requirement level. A number of electromagnetic effects cause test-mass disturbances, and each can be minimized to a considerable extent. Radiation pressure differences across the gravitational sensor housing are reduced by thermal isolation and making heat leaks as symmetrical as possible. Discharging the test-mass, reducing its displacement, and maximizing the test-mass-to-housing gap minimizes electric forces on the charged test mass. Fluctuating magnetic fields cause magnetic forces and, for a charged test mass, Lorentz forces. These forces are reduced by choosing a test-mass material with magnetic susceptibility of less than 10^{-6} and by discharging of the test mass.

The DRS drag-free test mass will be a cube of low magnetic susceptibility Au-Pt that is 4 cm on a side and has a mass of approximately 1.25 kg. A sample test mass has been machined from stainless steel, as shown in Figure 2. The surrounding housing will form a cubical cavity with a 2 mm gap between the test mass and the housing. Electrodes will be deposited on the sides of the housing as shown in Figure 3. One main electrode will be used to measure position in the direction of the second test mass, with a hole in the electrode for the laser beam used by the interferometer. To measure position and orientation, two electrodes are located on the 'top' and 'bottom' faces on the housing and four electrodes on the 'left' and 'right' side faces.

The capacitive measurement technology for position readout and attitude control of the test masses is based on the similar system used for GP-B. For GP-B, the test mass position is measured with capacitance bridges, using a 40 mV-PP 34 kHz sinusoidal sense signal superimposed onto the drive electrodes. The high-precision, low-noise design of the bridge results in an operational noise floor of $0.1 \text{ nm}/\sqrt{\text{Hz}}$, a resolution that allows the control system to meet the centering requirements for the GP-B mission. For DRS, to reduce force noise from the measurement system acting on the test mass, the position readout requirements will be relaxed to $3 \text{ nm}/\sqrt{\text{Hz}}$.

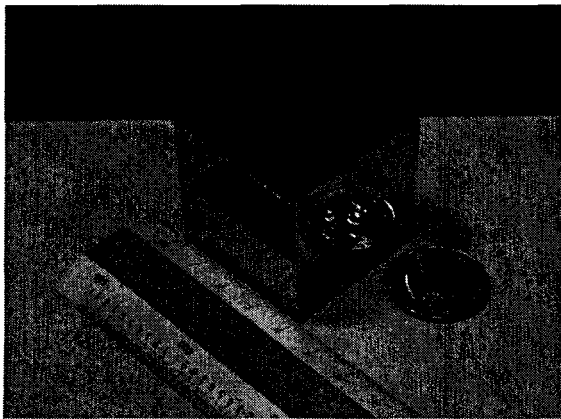


Figure 2 Prototype GRS test mass fabricated from stainless steel

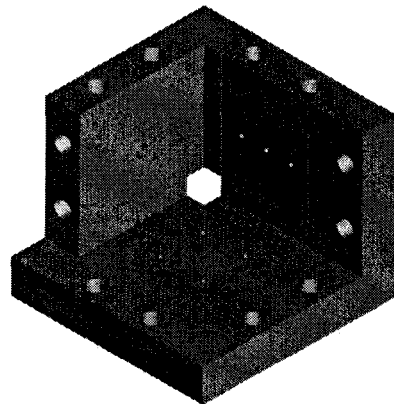


Figure 3 Electrode layout for GRS housing

3. COLLOIDAL MICROTHRUSTERS

The DRS requires microthrusters capable of smoothly varying thrust from 1 to 20 μN with 0.1 μN resolution and temporal stability for control of the position and attitude of the DRS spacecraft. The maximum thrust is determined by the need to counter the solar radiation pressure on the spacecraft. The thrust will be controlled with 0.1- μN resolution in order to control the spacecraft position with respect to the reference (test mass) within 10 nm/ $\sqrt{\text{Hz}}$. The microthrusters must smoothly and continuously counter all external disturbances, primarily solar pressure, with control authority over all 6 degrees of freedom of the spacecraft motion.

The DRS microthrusters consist of miniature ion engines. The propellant is a colloidal fluid, which is fed through a needle by a pressurizing system. At the tip of the needle, a high electrical field is applied, which causes droplets to form and to be ejected from the tip of the needle. The droplets are spontaneously ionized and accelerated by high voltage. Precise changes in thrust can be achieved by changes to the accelerating voltage. In order to prevent the spacecraft from becoming negatively charged by the continual ejection of positively-charged droplets, the microthrusters include a cathode to emit electrons to keep the spacecraft neutral.

Consider a small-diameter tube filled with low-volatility fluid, as shown in Figure 4. In general, the smaller the tube diameter the better, but practical considerations limit the tube inner diameter to some tens of microns. The fluid must be relatively nonvolatile to minimize its evaporation when exposed to the vacuum of space. It also should have electrical conductivity (K) that is a small fraction of 1 Si/m or greater (typical sea water has $K \approx 5$ Si/m). When sufficient voltage is applied between the extractor and the microtube (emitter), the liquid surface deforms into a cone, as sketched in Figure 4. Taylor³ found that this cone has a fixed angle of 49.3° , regardless of the type of fluid, its exact properties, or emitter geometry. Equilibrium on the surface of the cone is maintained by the balance of the liquid surface tension and electrostatic pressure. Near the tip, the electric field intensifies to a value that cannot be counteracted by the surface tension, and the cone tip transits into a small-diameter jet, which breaks up into charged droplets, which are accelerated to produce thrust.

A typical single emitter needle thruster produces a maximum thrust of 0.5 μN . To achieve larger thrust, multiple needles are needed. To achieve a thrust range of 1–20 μN requires variation of the acceleration voltage and variation of the flow rate. A prototype thruster system has been developed with an array of 52 emitters as shown in Figure 5.⁴ The system consists of the thruster, neutralizer, propellant feed system and the power-processing unit (PPU). The PPU contains all the DC-DC converters to power the system and the autonomous controls for the carbon nanotube field emission neutralizer. Figure 6 shows the overall thruster system schematic and Figure 7 shows the assembled prototype.

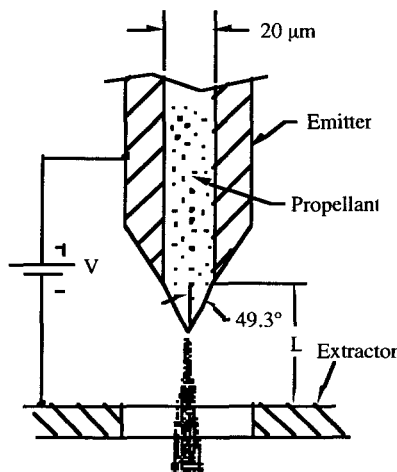


Figure 4 Schematic of the basic elements of a colloid thruster. A Taylor cone forms at the tip of the emitter upon application of sufficient voltage between the emitter and the extractor.

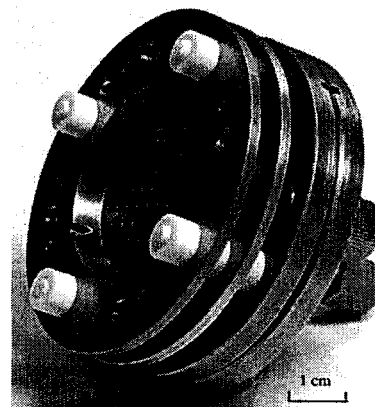


Figure 5 The 20- μN colloid thruster, which has 57 needles (nano droplet emitters), extractor grid, and an accelerator grid. The double grid is necessary to achieve the required thrust stability.

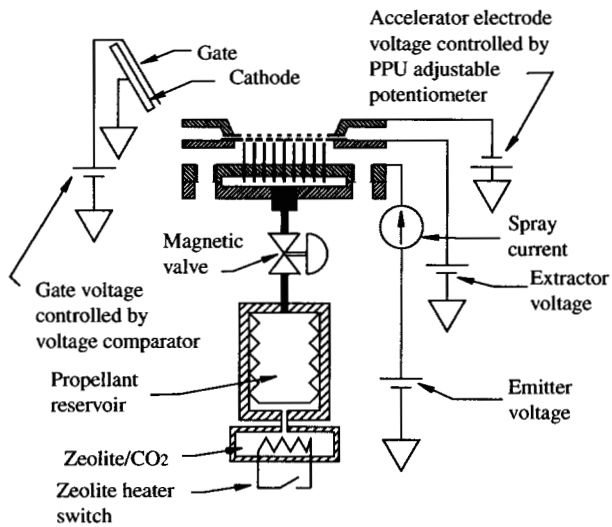


Figure 6 Schematic of the colloid thruster system

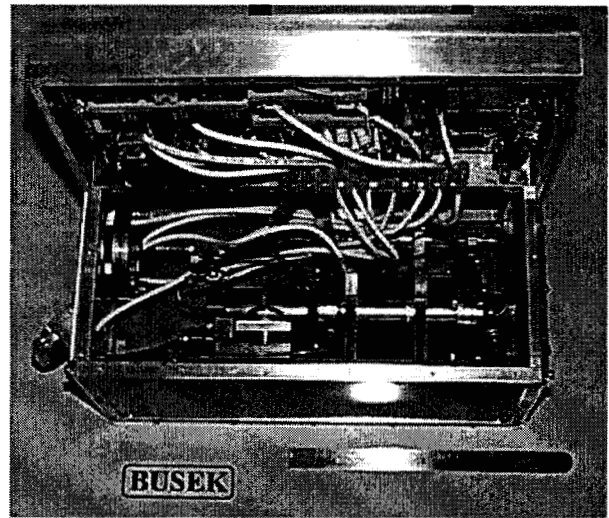


Figure 7 The 20- μN colloid thruster system during integration with the power-processing unit

The required low noise level on the thrusters is challenging to establish in ground tests. A special torsion balance test stand was developed to characterize the thrust output of a single colloidal thruster.⁵ Figures 8 and 9 show typical measured force output with the thruster initially off then commanded to a level of 0.11 μN and 0.88 μN . A test with the full scale microthruster system are planned for the next few months.

One issue to be addressed by the DRS space demonstration is the interaction of the charged propellant beam with the electronics emitted by the cathode to keep the spacecraft neutral. Beam neutralization is difficult to characterize in ground tests, since the high-velocity droplets interact with the sides of the test chambers and/or residual gas atoms that can neutralize the beam in the absence of the cathode. There is some chance that a charge distribution can form around the spacecraft that will interfere with the performance of the thrusters. This will be tested by using the gravitational reference sensors to measure the acceleration produced by the thrusters over many days to look for variation in output. Contamination is another issue that will be addressed. Because the propellant vaporizes at room temperature, and is emitted at high velocity, contamination is expected to be low.

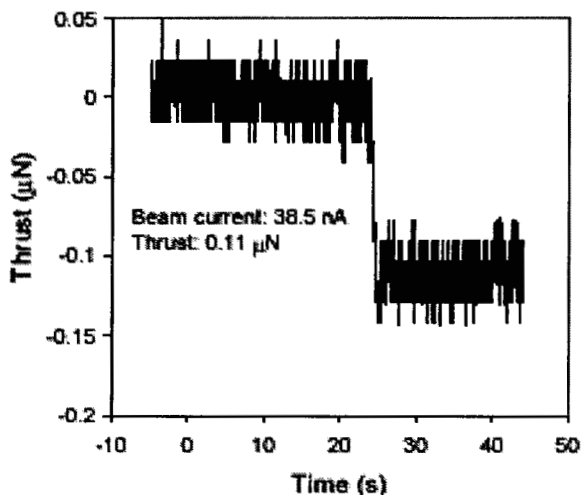


Figure 8 Measured response for thrust step of 0.11 μN

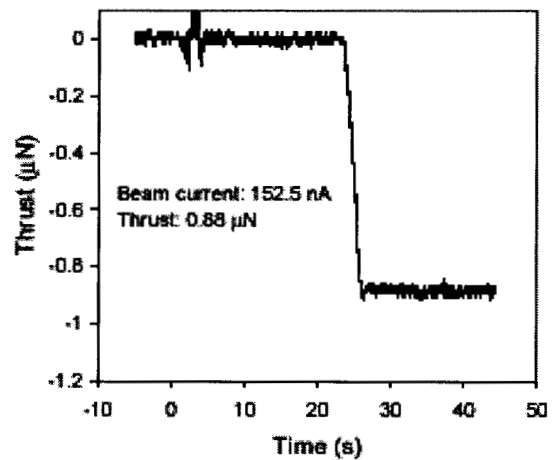


Figure 9 Measured response for thrust step of 0.88 μN

4. PRELIMINARY CONTROL SYSTEM SIMULATION RESULTS

In order to develop a preliminary control system design to help determine the required position measurement and thrust control noise, a one-dimensional model was developed. The model includes a test mass free to move in the x direction, surrounded by a spacecraft with one thruster to oppose a force due to solar radiation pressure. The test mass was assumed to have an intrinsic acceleration noise of $3 \times 10^{-14} \text{ m/s}^2/\sqrt{\text{Hz}}$ over the frequency range of 1 mHz to 10 mHz, increasing as $1/f$ for lower frequencies. The position of the test mass was measured with respect to the test mass with noise $3 \text{ nm}/\sqrt{\text{Hz}}$. No force coupling between spacecraft and test mass was included. The force on the spacecraft from the sun was assumed to have a noise due to variation in solar output as measured by the SOHO spacecraft.⁶ The thrusters were assumed to have a noise of $0.1 \text{ } \mu\text{N}/\sqrt{\text{Hz}}$. For some tests the thrusters were assumed to be continuously adjustable, while in others the effect of a discrete step size of $0.1 \text{ } \mu\text{N}$ was included. A key parameter of interest was the control loop update rate, since this will affect the instrument development and required computing resources. The thruster dynamic range is also of interest, since large changes in thrust require changes in propellant pressure, which potentially has a slower response time than acceleration voltage changes which can be used to make small adjustments in thrust output.

Figure 10 shows the simulated spacecraft position as a function of time over several thousand seconds. Figure 11 shows a 10 second sample of Figure 10 with fined resolution. The results show that the spacecraft position is well controlled at the nanometer level.

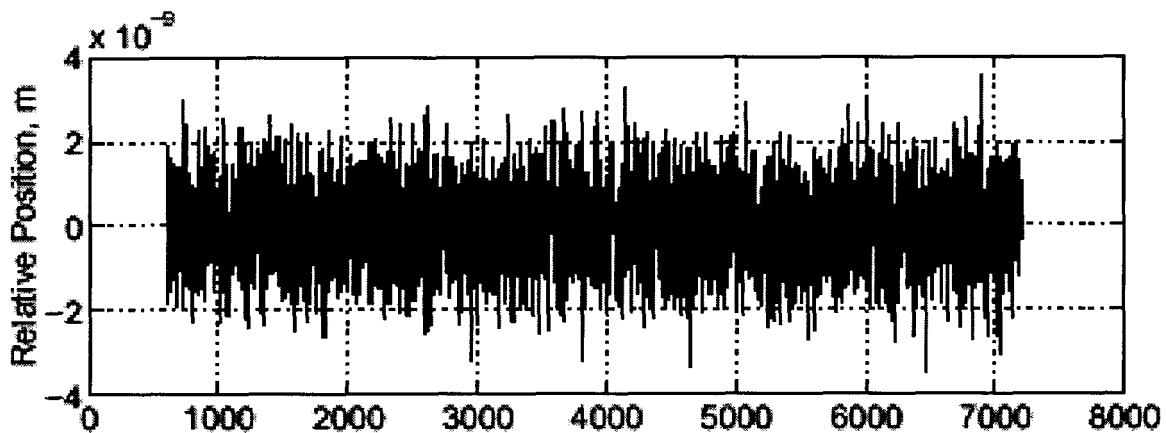


Figure 10 Position of spacecraft versus time with 10 Hz control rate

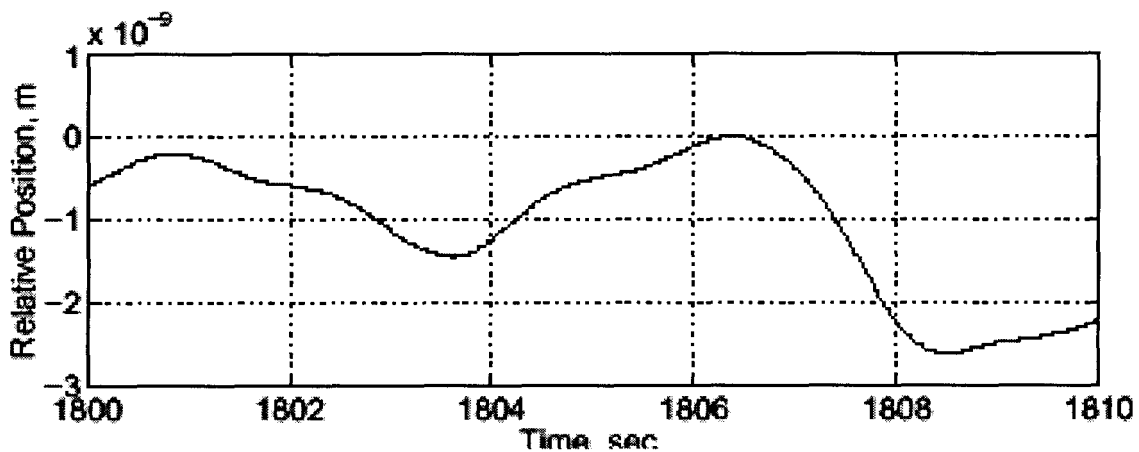


Figure 11 Position of spacecraft versus time with 10 Hz control rate

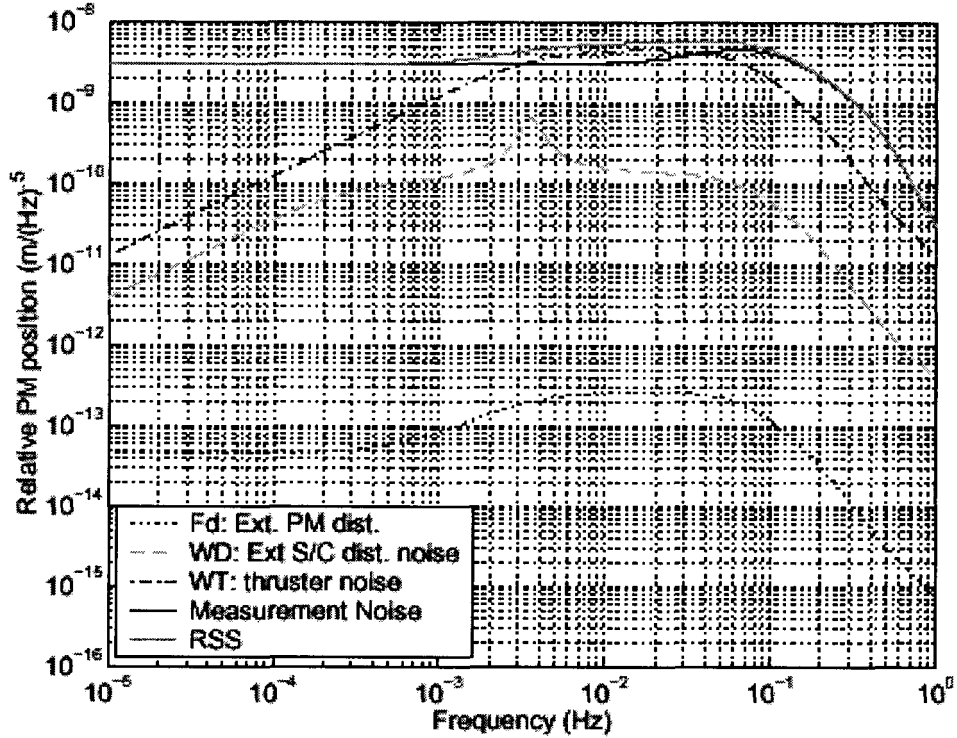


Figure 12 Power spectrum of the spacecraft position relative to the test mass

Figure 12 shows the power spectral density of the spacecraft position, with contributions from the various noise source. Within the primary frequency band of interest, 1 mHz to 10 mHz, the position sensing noise and thruster noise have comparable effect, with the overall total meeting the requirement of 10 nm/ $\sqrt{\text{Hz}}$. The effect of solar pressure fluctuations is much smaller, and the noise due to the motion of the test mass is negligible as far as spacecraft control is concerned.

Figure 13 shows a part of the time series of the commanded thrust required for the spacecraft position control model. The effect of discrete thrust commands is evident. In other tests, the effect of the finite thrust command size did not contribute significantly to the position control noise as long as the step size was less than 0.4 μN . The required thrust variation is about $\pm 5\%$ of the nominal value, which is compatible with the range of thrust achievable with voltage control of the colloidal thrusters.

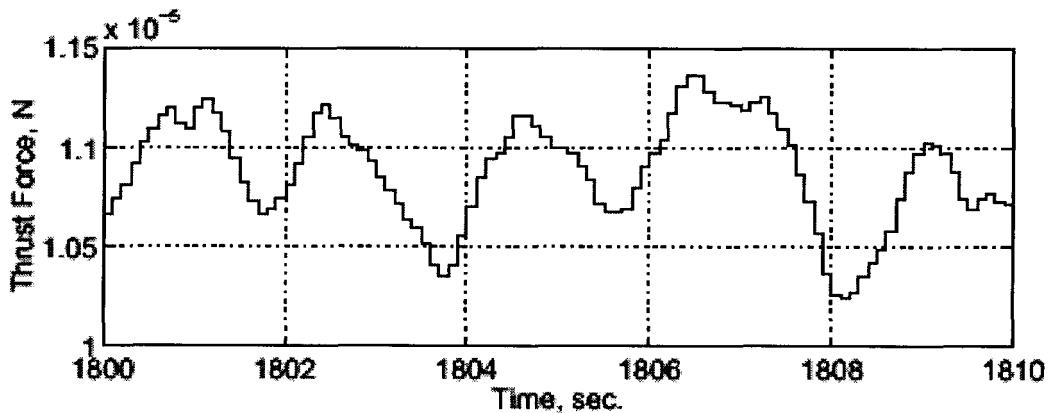


Figure 13 Commanded thrust versus time for the 10 Hz spacecraft position control model.

5. FUTURE PLANS

In the next few month the DRS team will be performing design development and initial performance tests. Enhanced simulations are planned which will include full three-dimensional simulation with two test masses and 18 degrees of freedom control. Tests of the prototype thruster with its array of 52 needles are planned to measure its thrust output over longer periods of time, and evaluation of expected contamination levels.

6. ACKNOWLEDGEMENTS

The research described in this paper was, in part, carried out by the Jet Propulsion Laboratory, California Institute of Technology, under a contract with the National Aeronautics and Space Administration.

7. REFERENCES

1. Space Science Dept of Joohns Hopkins Applied Physics Laboratory and Guidance and Control Department of Stanford University, "A satellite freed of all but gravitational forces: Triad", *J. Spacecraft* **11**, 637-644, 1974
2. J. P. Turneure, C. W. F. Everitt, B. W. Parkinson, *Advances in Space Research*, **9**, 29 (1989).
3. Taylor, G.I., "Disintegration of water drops in an electric field", *Proc. R. Soc., London A* **280**, 383-397
4. M. Gamero-Castaño & V. Hruby, "Electrospray as a source of nanoparticles for efficient colloid thrusters". *Journal of Propulsion and Power*, to be published in Vol. 7, No. 4, July 2001.
5. M. Gamero-Castaño and V. Hruby, *IEPC-01-235*, 2001
6. J. Pap et al., "Variation in total solar and spectral irradiance as measured by the VIRGO experiment on SOHO", *Adv. Space Res.* **24**, 215-224, 1999.